Contents lists available at ScienceDirect

# Journal of Non-Newtonian Fluid Mechanics

# Turbulent pipe flow of a drag-reducing rigid "rod-like" polymer solution

A. Japper-Jaafar, M.P. Escudier, R.J. Poole *

*Department of Engineering, University of Liverpool, Brownlow Street, Liverpool, L69 3GH United Kingdom*

## ARTICLE INFO

## ABSTRACT

Fully developed turbulent pipe flow of an aqueous solution of a rigid "rod-like" polymer, scleroglucan, at concentrations of 0.005% (w/w) and 0.01% (w/w) has been investigated experimentally. Fanning friction factors were determined from pressure-drop measurements for the Newtonian solvent (water) and the polymer solutions and so levels of drag reduction for the latter. Mean axial velocity $u$ and complete Reynolds normal stress data, i.e. $u'$, $v'$ and $w'$, were measured by means of a laser Doppler anemometer at three different Reynolds numbers for each fluid. The measurements indicate that the effectiveness of scleroglucan as a drag-reducing agent is only mildly dependent on Reynolds number. The turbulence structure essentially resembles that of flexible polymer solutions which also lead to low levels of drag reduction.

## 1. Introduction

The phenomenon of drag reduction, often referred to as "Tom's phenomenon", has been the subject of extensive reviews by Lumley [1], Virk [2], Berman [3], Hoyt [4], Nieuwstadt and den Toonder [5], Graham [6] and many others, and the behaviour of flexible polymer solutions as drag-reducing agents is now fairly well understood. A notional limit of drag reduction of 40% has been found below which, the flow is categorized as "low" drag-reducing and above which, "high" drag-reducing (e.g. Warholic et al. [7] and Escudier et al. [8]). There are marked differences between these two categories. For "low" drag-reducing flows, the normalized mean velocity in law-of-the-wall form ($u^+$) remains parallel to the Newtonian data but is upshifted [7,8]. In addition, the peak value of the normalized axial velocity fluctuations ($u'^+$) increases, the peak values of the radial ($v'^+$) and tangential ($w'^+$) velocity fluctuations decrease together with a monotonic decrease of the Reynolds shear stress ($\rho\overline{u'v'}$) [7]. Different trends are observed for high drag-reducing flows where there is a significant increase in the slope of the universal mean velocity profile [7]. At such high levels of drag reduction the normalized axial velocity fluctuation levels are ultimately suppressed with concomitant decreases of the Reynolds shear stress, to almost zero levels close to the maximum drag reduction asymptote [2], with corresponding increases in the so-called "polymer stress".

The drag-reducing mechanisms of "rigid" or "rod-like" polymers are far from as well studied or understood as is the case for flexible polymers. The limited literature on these polymers has shown

that the polymer solutions are also capable of drag reduction but possibly to a lesser degree than flexible polymer solutions (e.g. the boundary-layer (polymer injection) work of Paschkewitz et al. [9]). However, while high molecular weight flexible polymer solutions are very prone to mechanical degradation, an advantage of rigid polymer solutions is that they are more resistant (Paschkewitz et al. [9], Hoyt [4]). An additional advantage of rigid polymers is that they tend to be biopolymers, derived through biological fermentation.

Berman [3] found that rigid structures and polyelectrolytes were not effective drag reducers until the concentration was "high enough" which was also confirmed by his later study [10]. Using collagen and carrageenan, the ratio of circumscribed volume of the molecules to the actual volume (the lengths of the rod-like molecules were used as diameters to calculate the circumscribed volume) was found to be at least 30 for the solution to be drag-reducing. Through pressure-drop measurements it was observed that the rigid polymer solutions were drag-reducing but did not show any drag reduction onset (i.e. there appeared to be no critical wall shear stress before drag reduction occurred). Although exhibiting drag reduction, the slopes of the friction factor, $f$, against the Reynolds number, $Re$, plotted in log–log coordinates remained parallel to that for the Newtonian fluid flow. In contrast to polyelectrolytes and flexible polymer solutions, no diameter effect was observed for these rigid polymer solutions [10].

Bewersdorff and Singh [11] studied the drag reduction of xanthan gum solutions, in which molecule rigidity was varied by the addition of salt to increase flexibility. Without salt addition, the $f$–$Re$ data of the xanthan gum solutions (again plotted in log–log coordinates) exhibited drag reduction but the curves remained parallel to that for the Newtonian fluid. The greater flexibility due to the addition of salt resulted in greater drag reduction. These results are in disagreement with the observations of both Sasaki [12] and Virk et

* Corresponding author. Fax: +44 151 7944848.
*E-mail addresses:* a.jaafar@liv.ac.uk (A. Japper-Jaafar),
escudier@liv.ac.uk (M.P. Escudier), robpoole@liv.ac.uk (R.J. Poole).

## Nomenclature

| | |
|---|---|
| $a$ | Carreau–Yasuda parameter |
| $b$ | diameter of CaBER plates (4 mm) |
| $c$ | polymer concentration (%, w/w) |
| $c^*$ | critical overlap concentration (%, w/w) |
| $D$ | pipe diameter (m) |
| $D_{CaBER}$ | filament diameter in CaBER (mm) |
| $D_o$ | midpoint filament diameter in CaBER following cessation of stretch deformation (mm) |
| DR | drag reduction (%), $\left(\equiv (f_n - f_p)/f_n \times 100\right)$ |
| $f$ | Fanning friction factor, $(\equiv 2\tau_W/\rho U_B^2)$ |
| $G'$ | storage modulus (Pa) |
| $G''$ | loss modulus (Pa) |
| $h$ | distance between plates in CaBER (mm) |
| $L$ | pipe length over which the pressure drop was measured (m) |
| $m$ | slope of linear fitting to CaBER data (mm/s) |
| $n$ | power-law index |
| $\Delta p$ | pressure drop (Pa) |
| $\dot{Q}$ | volumetric flowrate (m$^3$/s) |
| $Re$ | Reynolds number $(\equiv \rho U_B D/\eta_W)$ |
| $t$ | time (s) |
| $T_B$ | filament breakup time in CaBER (s) |
| $Tr$ | Trouton ratio, $(\equiv \eta_E(\sqrt{3}\dot{\varepsilon})/\eta(\dot{\gamma}))$ |
| $u$ | mean axial velocity (m/s) |
| $u^+$ | mean axial velocity normalised by friction velocity $(\equiv u/u_\tau)$ |
| $u_\tau$ | friction velocity (m/s), $(\equiv \sqrt{\tau_W/\rho})$ |
| $u'$ | RMS axial velocity fluctuation (m/s) |
| $u'^+$ | RMS axial velocity fluctuation normalised by friction velocity $(\equiv u'/u_\tau)$ |
| $\overline{u'v'}$ | Reynolds shear stress (m$^2$/s$^2$) |
| $U_B$ | bulk velocity (m/s), $(\equiv 4\dot{Q}/(\pi D^2))$ |
| $v'$ | RMS radial velocity fluctuation (m/s) |
| $v'^+$ | RMS radial velocity fluctuation normalised by friction velocity $(\equiv v'/u_\tau)$ |
| $w'$ | RMS tangential velocity fluctuation (m/s) |
| $w'^+$ | RMS tangential velocity fluctuation normalised by friction velocity $(\equiv w'/u_\tau)$ |
| $y$ | distance from pipe wall (m) |
| $y^+$ | distance from pipe wall normalised by friction velocity $(\equiv \rho y u_\tau/\eta_W)$ |

*Greek letters*

| | |
|---|---|
| $\dot{\gamma}$ | shear rate (1/s) |
| $\dot{\gamma}_W$ | shear rate at the wall (s$^{-1}$) |
| $\dot{\varepsilon}$ | strain rate determined from CaBER (1/s), $\left(\equiv -\frac{4}{D_o}\frac{dD_{CaBER}}{dt}\right)$ |
| $\eta$ | shear viscosity (Pa s) |
| $\eta_E$ | uniaxial extensional viscosity (Pa s) |
| $\eta_o$ | zero-shear rate viscosity (Pa s) |
| $\eta_W$ | wall shear viscosity obtained from $\tau_W$ and $\dot{\gamma}_W$ via Carreau–Yasuda fit (Pa s) |
| $\eta_\infty$ | infinite-shear rate viscosity (Pa s) |
| $\lambda$ | characteristic relaxation time in CaBER (s) |
| $\lambda_{CY}$ | Carreau–Yasuda constant representing onset of shear thinning (s) |
| $\rho$ | fluid density (kg/m$^3$) |
| $\tau_W$ | wall shear stress (Pa) $(\equiv \Delta p D/4L)$ |
| $\omega$ | angular frequency (rad/s) |

*Subscripts*

| | |
|---|---|
| N | Newtonian |
| P | polymer |
| W | wall |

*Superscripts*

| | |
|---|---|
| + | "wall" coordinates |

al. [13] however. Virk et al. [13] found that increasing the flexibility of hydrolyzed polyacrylamide reduced the drag reduction ability of the polymer solution. Sasaki [12] also studied the drag-reducing ability of what he termed a "strictly rigid" polymer solution, scleroglucan, and found the trend to be in close agreement with that of a semi-rigid xanthan gum solution without salt addition.

Benzi et al. [14] postulated through theoretical considerations that the slope of the maximum drag reduction asymptote (*f–Re* plot) discovered by Virk [2] applies to both flexible and rigid polymers. However, their work showed that the dynamics of these polymers upon approaching the asymptote are different. They found that the degree of drag reduction for a rigid polymer is dependent only on the concentration while it is well known that for a flexible polymer, it is a function of concentration, Reynolds number and the Deborah number [1–5]. For flexible polymers, the asymptote is reached even for low concentrations and then a crossover back to the Newtonian core is found. For rigid polymers, maximum drag reduction is approached gradually as concentration is increased. Paschkewitz et al. [15] conducted direct numerical simulations of non-Brownian fibres (no elasticity) in a turbulent channel flow. At 15% drag reduction, the mean axial and turbulence structure data are found to be similar to that of low drag-reducing flexible polymer solutions leading to the conclusion that elasticity is not necessary for drag reduction. The Reynolds shear stress is reduced throughout the entire channel and the polymer stress shows large values closer to the wall suggesting that fibres most strongly affect the flow in the near-wall region ($y^+ < 100$). Similar observations were also made by Benzi et al. [16]. The drag reduction effectiveness is also found to increase with increasing aspect ratio of the fibres (Paschkewitz et al. [15], Gillissen et al. [17]).

To date, with the notable exception of the boundary-layer experiments of Paschkewitz et al. [9], there is no experimental information on the mean velocity and on the turbulence statistics of rigid polymer solutions in fully developed pipe flow, or indeed any pure shear flow. The present paper aims to address this deficit by studying the effects of concentration and Reynolds number on the degree of drag reduction of a "strictly rigid" polymer solution, scleroglucan, in a large-scale circular pipe flow facility (i.e. the same polymer as studied in [9] and [12]). Measurements on the Newtonian solvent, at Reynolds numbers close to that of the polymer solution flow, were also performed for comparison. As has been pointed out by den Toonder and Nieuwstadt [18] the turbulent fluctuation components for Newtonian pipe flow, normalized with the friction velocity ($u_\tau$), are Reynolds number dependent. Hence, it is important, as we ensure here, that the flow measurements for the Newtonian fluid are conducted at the same Reynolds number as that of the polymer solutions. The Reynolds number is defined here based on the bulk velocity, pipe diameter and the fluid viscosity at the wall ($Re = \rho U_B D/\eta_W$).

## 2. Experimental arrangement

The measurements were carried out in a 23-m long circular pipe flow facility, which is essentially an extended version of the flow loop described in detail in [19] (Fig. 1). The test pipe (1) comprised of
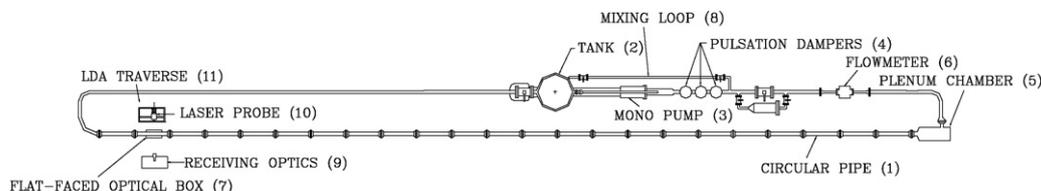
**Fig. 1.** Schematic diagram of the flow loop.

21 precision-bore borosilicate glass tubes, each about $1029 \pm 2$ mm long, a single glass tube 656 mm in length and one PVC plastic pipe, 1060 mm long, at the test section entrance. The internal diameter of the tubes is $100.4 \pm 0.1$ mm. The fluid was driven from a 500-l capacity stainless steel tank (2) by a progressive cavity pump (3) (Monotype, E101 with a maximum flowrate of 0.025 m³/s). Three pulsation dampers (4) located immediately after the pump outlet acted to remove pulsations resulting from the rotation of the mono pump. A cylindrical plenum-chamber (5) upstream of the pipe test section minimizes swirl and suppresses disturbances with the intention of providing a smooth uniform inflow into the pipe. A Coriolis mass flowmeter (6) (Promass 63, manufactured by Endress + Hauser) was also incorporated in the experimental rig. The pressure drop was measured by means of a differential pressure transducer, GE Druck (LPX9381) with a range of 5000 Pa and an uncertainty of less than 1.5%, over a distance of 7.2 m (72 D) starting 14 m (140 D) downstream of the inlet. Readings of the transducer under no-flow conditions were made at the beginning and end of each measurement to account for any drift where the zero flowrate readings were monitored and subsequent readings were corrected accordingly.

Mean velocity profiles and turbulent fluctuation levels, were measured 22 m (220 D) downstream of the inlet of the pipe test section, using a Dantec Fiberflow laser Doppler anemometer (LDA) system comprising of a 60X10 probe and a Dantec 55X12 beam expander in conjunction with a Dantec Burst Spectrum Analyzer signal processor (model 57N10). The lens focal length is 160 mm and the measured half angle between the laser beams is 8.4° which produces a measuring volume with a diameter of 40 μm and a length of 0.27 mm in air, calculated using the procedure of Buchhave et al. [20]. The axial and tangential velocities and the respective radial locations were corrected as suggested by Bicen [21]. The radial velocity measurements were conducted with a flat-faced optical box (7), filled with water, placed on the test section to minimize the amount of refraction of the beams making it possible to obtain data closer to the wall. The radial velocities and locations were corrected using the ray-tracing method outlined by Presti [22].

At each radial location 10,000–20,000 data samples were collected and processed using a simple ensemble-averaging method. Processing the data using a transit-time weighting method [23] to account for velocity-biasing effects produced minimal differences compared with processing the data using a simple ensemble-averaging method (differences of less than 2% in the RMS fluctuation levels). The maximum statistical error, for a 95% confidence interval, was less than 0.5% in mean velocity and less than 1.5% in the turbulence intensity based on the method of Yanta and Smith [24]. The flowrates obtained from integration of the LDA mean velocity profiles were found to be within 1.5% of the value provided by the flowmeter.

Approximately 700 l of tap water was used as the solvent for the test fluid. Mixing of part of the solvent with the polymer powder was achieved by recirculating the polymer solution within the mixing loop (8) at a low pump speed for at least 5 h before the mixing loop was opened and the solution was circulated in the flow loop, allowing further mixing with the rest of the solvent in the pipe for at least another 5 h, until the solutions appeared to be visibly homogeneous. The homogeneity of the solution was also checked by comparing the viscometric data with a small sample solution prepared separately of the same concentration. Formaldehyde was added to the polymer solution at a concentration of 100 ppm to retard bacteriological degradation. The polymer solution was then left to hydrate in the rig for at least 24 h prior to commencing the LDA measurement. Measurements of fluid rheology were conducted prior to and after each LDA profile to check for signs of mechanical and bacteriological degradation. In order to increase the signal-to-noise ratio and the data rate for the LDA measurements, seeding particles (Timiron MP1005, mean diameter ≈5 μm) were added at a concentration of about 1 ppm.

## 3. Working fluid characterization

The scleroglucan (Actigum™ CS, provided by Cargill Incorporated and hereafter referred to as SG) used in this study is a non-ionic polysaccharide produced by the fungi of genus Sclerotium with a molecular weight reported by the supplier to be about $5.4 \times 10^5$ g/mol. The rigid structure of the polymer is attributable to the long persistence length ([25]) of the molecule originating from its triple helical structure ([12,9]).

Steady-shear measurements and small-amplitude oscillatory-shear measurements (SAOS) were conducted over a wide range of concentrations (0.005–0.5% (w/w) for steady-shear and 0.075–0.5% (w/w) for SAOS) at 20 °C using a TA-Instruments Rheolyst AR 1000 N controlled-stress rheometer. The plot of shear viscosity against shear rate in Fig. 2 shows increased dependence of the shear viscosity, $\eta$ on shear rate, $\dot{\gamma}$ with increasing concentration, i.e. increased shear thinning. The Carreau–Yasuda model ([26]) was used to fit the data

$$\frac{\eta - \eta_0}{\eta_0 - \eta_\infty} = \frac{1}{[1 + (\lambda_{CY}\dot{\gamma})^a]^{n/a}} \tag{1}$$
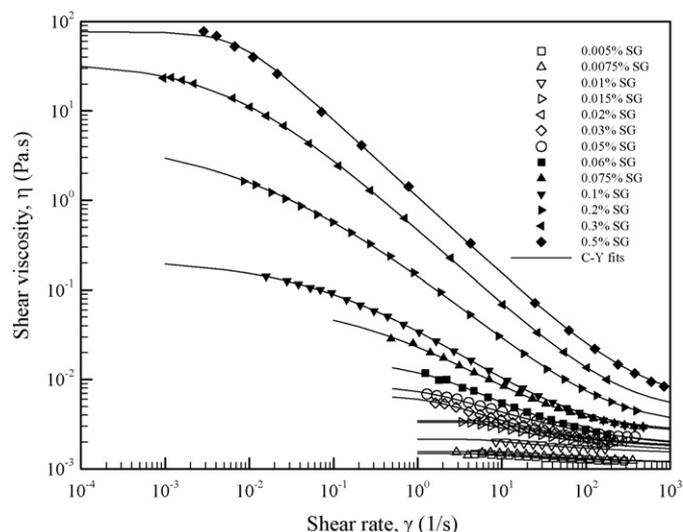


**Fig. 2.** Viscometric data for various scleroglucan concentrations together with the Carreau–Yasuda fits.

**Table 1**
Carreau–Yasuda parameters for scleroglucan solutions.

| Scleroglucan concentration, $c$ % (w/w) | Zero-shear viscosity, $\eta_o$ (Pa s) | Infinite-shear viscosity, $\eta_\infty$ (Pa s) | Constant which represents onset of shear thinning, $\lambda_{CY}$ (s) | Power-law index, $n$ | Carreau–Yasuda parameter, $a$ |
|---|---|---|---|---|---|
| 0.005 | $1.48 \times 10^{-3}$ | $1.12 \times 10^{-3}$ | $1.70 \times 10^{-1}$ | 0.30 | 5.82 |
| 0.0075 | $1.56 \times 10^{-3}$ | $1.12 \times 10^{-3}$ | $1.71 \times 10^{-1}$ | 0.31 | 5.84 |
| 0.01 | $2.14 \times 10^{-3}$ | $1.41 \times 10^{-3}$ | $1.73 \times 10^{-1}$ | 0.31 | 5.78 |
| 0.015 | $3.33 \times 10^{-3}$ | $1.49 \times 10^{-3}$ | $2.04 \times 10^{-1}$ | 0.42 | 5.63 |
| 0.02 | $3.45 \times 10^{-3}$ | $1.67 \times 10^{-3}$ | $1.26 \times 10^{-1}$ | 0.50 | 5.15 |
| 0.03 | $6.59 \times 10^{-3}$ | $1.73 \times 10^{-3}$ | $6.17 \times 10^{-1}$ | 0.55 | 1.62 |
| 0.05 | $8.48 \times 10^{-3}$ | $1.74 \times 10^{-3}$ | $7.21 \times 10^{-1}$ | 0.47 | 1.27 |
| 0.06 | $1.52 \times 10^{-2}$ | $1.73 \times 10^{-3}$ | $8.19 \times 10^{-1}$ | 0.59 | 1.24 |
| 0.075 | $7.42 \times 10^{-2}$ | $2.51 \times 10^{-3}$ | $2.08 \times 10^{0}$ | 0.73 | 0.90 |
| 0.1 | $2.24 \times 10^{-1}$ | $2.59 \times 10^{-3}$ | $5.01 \times 10^{0}$ | 0.78 | 0.55 |
| 0.2 | $5.33 \times 10^{0}$ | $3.07 \times 10^{-3}$ | $4.99 \times 10^{1}$ | 0.82 | 0.45 |
| 0.3 | $3.48 \times 10^{1}$ | $4.22 \times 10^{-3}$ | $1.46 \times 10^{2}$ | 0.86 | 0.62 |
| 0.5 | $7.70 \times 10^{1}$ | $5.53 \times 10^{-3}$ | $1.37 \times 10^{2}$ | 0.87 | 1.86 |

where $\eta_o$ and $\eta_\infty$ are the viscosities in the zero-shear and infinite-shear plateaus while $\lambda_{CY}$, $n$ and $a$ are constants which represents the inverse shear rate at the onset of shear thinning, the power-law index and a parameter introduced by Yasuda et al. [26], respectively. Table 1 lists the Carreau–Yasuda parameters for the fits. These model parameters were obtained using the methodology of Escudier et al. [27].
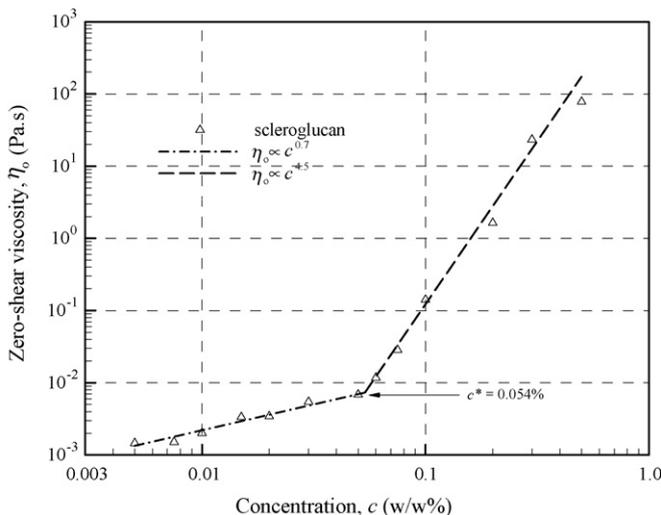
A plot of zero-shear rate viscosity, $\eta_o$, against the solution concentration, $c$ (Fig. 3), provides a way of estimating the critical overlap concentration, $c^*$, which is regarded as the point at which individual polymer molecules begin to interact with each other ([25]), and for this particular scleroglucan is about 0.054% (540 ppm).

Fig. 4 shows the storage ($G'$) and loss ($G''$) moduli plotted against frequency for higher solution concentrations ($c \geq 0.075\%$) measured in SAOS. Data for lower concentrations are not included as the $G'$ data fell within 50% of the instrument/geometry limit data. The limit data was based on an oscillatory test conducted on water: non-zero values of $G'$ obtained in such a test are a consequence of inertia and represent a limit of the instrument. As shown, the loss modulus, $G''$ is greater than the elastic modulus $G'$ prior to the crossover for the lower concentration solutions. The crossover frequency decreases with concentration indicating viscous dominance at low concentrations compared to that at high concentrations. For the 0.5% solution, the elastic component plays a dominant role, at least for the frequency range tested. The dependence of both moduli on frequency reducing with concentration is indicative of structure
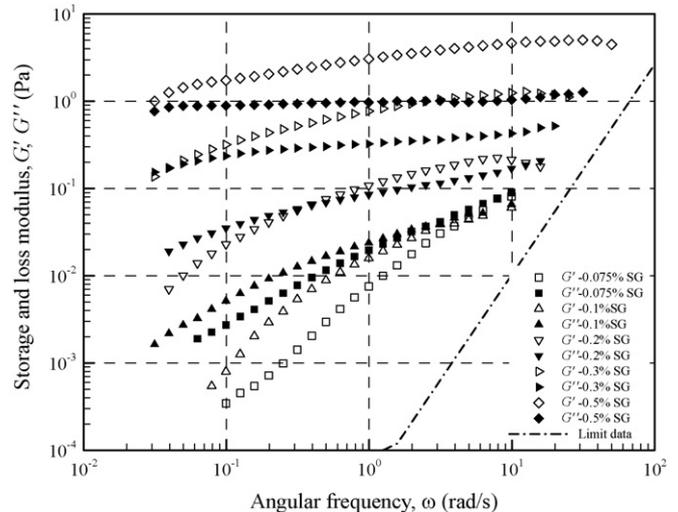
build-up as suggested by Rochefort and Middleman [28] and Lee [29]. At the highest concentration (0.5%) the solution is essentially gel-like.

Much as was the case for the SAOS data, extensional property measurements were only possible for higher concentration solutions ($c \geq 0.1\%$) and were carried out using a Capillary Break-up Extensional Rheometer ("CaBER") supplied by Thermo Electron GmbH in conjunction with a high-speed camera. The CaBER utilizes a laser micrometer, with a resolution of around 10 μm, to monitor the diameter of the thinning elongated filament, which evolves under the action of viscous, inertia, gravitational and elastocapillary forces. High-speed digital imaging of the process was captured by a Dantec Dynamics Nano Sense MKIII high-speed camera with a Nikon 60 mm f/2.8 lens at 2000 frames per second.
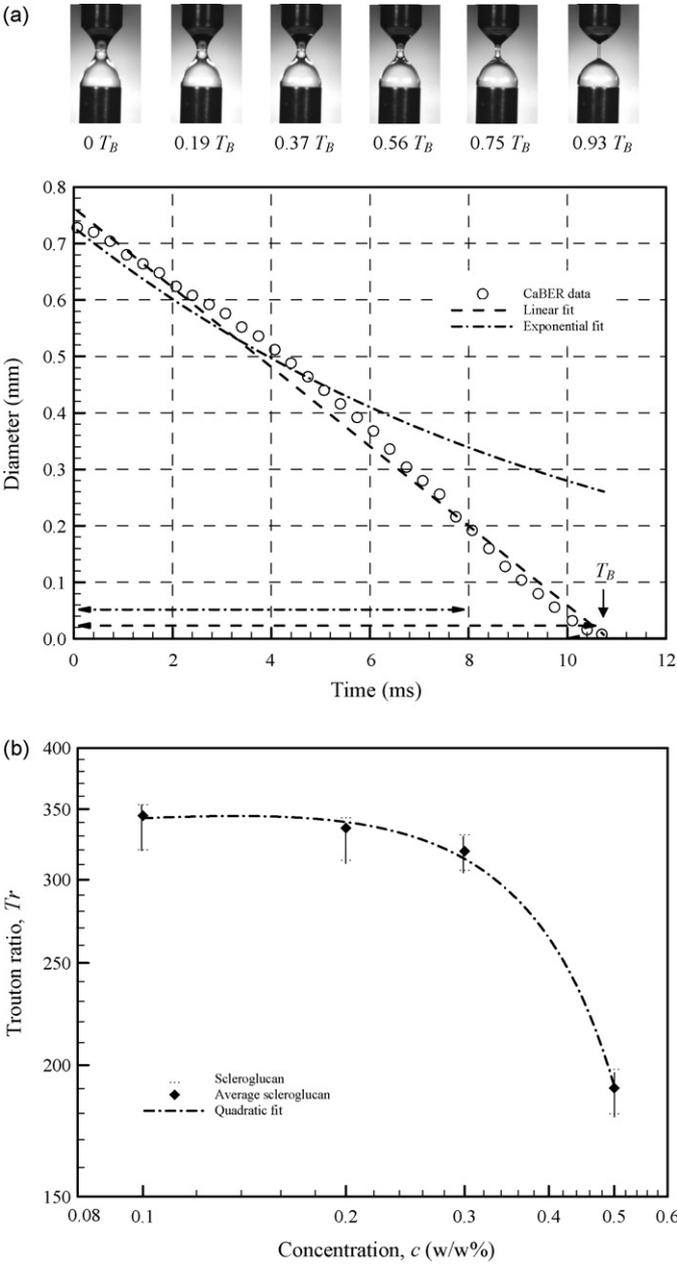
A sample of about 25 mm³ was loaded using a syringe between the 4 mm plates of the instrument, making sure that it was totally homogeneous with no bubbles within the sample. The initial aspect ratio ($\equiv h/b$) of 0.5 was chosen based on the recommendation by Rodd et al. [30] to minimize the effects of reverse squeeze flow and sagging. A uniaxial step strain was then applied, resulting in the formation of an elongated filament. A linear stretching deformation was employed as the mode of the step strain. The stretch time was set to 50 ms. The final aspect ratio was varied with solution concentration such that filament thinning was still observed between the 4 mm plates. For example, a final aspect ratio of 1.4 was chosen for 0.1% SG in order to observe filament thinning over a timeframe of about 10 ms.

**Fig. 3.** Zero-shear viscosity versus SG concentration.

**Fig. 4.** Storage ($G'$) and loss ($G''$) modulus versus angular frequency ($\omega$) for various SG concentrations.

Fig. 6. f–Re data for various SG concentrations.

$$T_r = \frac{\eta_E(\sqrt{3}\dot\varepsilon)}{\eta(\dot\gamma)} \tag{4}$$

with the strain rate calculated from

$$\dot\varepsilon = -\frac{4}{D_o}\frac{dD_{CaBER}}{dt} \tag{5}$$

Newtonian linear thinning was observed over the entire time to breakup with a slope of about 70 mm/s. Linear fitting the last six data points prior to breakup, where the sample most closely resembles the uniform cylindrical shape used in deriving Eqn. (2) and (3), gave a slope within 10% of the global fit. Linear thinning was also observed for higher concentrations. Despite this apparent Newtonian behaviour, the Trouton ratio plotted against concentration in Fig. 5(b) confirms the non-Newtonian behaviour of this scleroglucan as the magnitude for all the concentrations studied was significantly greater than that of a Newtonian fluid, i.e. $T_r \gg 3$. Although, due to instrument limitations, CaBER data could not be obtained for concentrations at which the fluid-dynamic measurements were carried out, it can be seen that across a wide range of concentration (0.1–0.3%) the Trouton ratio remains approximately constant at a value of $340 \pm 10$.

## 4. Pressure-drop measurements

The Fanning friction factor, $f$ ($\equiv 2\tau_W/\rho U_B^2$) is plotted against Reynolds number $Re$ for a wide range of concentrations (0.005–0.075%) in Fig. 6. The Reynolds number is defined based on the bulk velocity, pipe diameter and the shear viscosity at the wall ($Re \equiv \rho U_B D/\eta_W$). The wall viscosity, $\eta_W$ was obtained from the Carreau–Yasuda model fit [26] to the steady-shear viscosity measurements, using the wall shear stress determined from the pressure-drop measurements. Due to the low viscosity of most of the solutions, especially those for which $c < c^*$, laminar flow conditions were not attainable within the operating range of the flow loop. The majority of pressure-drop measurements taken were therefore limited to the turbulent regime and little information could be gleaned regarded transitional Reynolds numbers. The friction factors show increased deviations with increasing concentration from those of the Newtonian solvent (water) towards Virk's "maximum drag reduction asymptote" (Virk [2])

$$f = 0.58Re^{-0.58} \tag{6}$$

The drag reduction figures quoted in Table 2 at several Reynolds numbers, are calculated based on the friction factor of the poly-

Fig. 5. (a) Filament diameter thinning as a function of time for 0.1% SG at 20 °C (arrow lines represent the time period for exponential fit (−·−) and linear fit (−−)) (b) Trouton ratio versus SG concentration (fit is provided to guide the eye). The error bars represent data variations calculated from at least four measurements.

Fig. 5(a) shows the decay of the filament diameter against time for 0.1% SG which was fitted to an equation of the form

$$D_{CaBER} = D_o e^{-t/3\lambda} \tag{2}$$

as recommended by Stelter and Brenn [31] for viscoelastic fluids, where $D_o$ is the midpoint diameter following cessation of the stretch deformation and $\lambda$ is a characteristic relaxation time which represents the characteristic time scale for viscoelastic stress growth in uniaxial elongational flow ([30]). A linear fitting characteristic of "Newtonian-like" thinning

$$D_{CaBER} = mt + D_o \tag{3}$$

was also fitted to the data. The Trouton ratio was calculated using the equation recommended by Pelletier et al. [32]

**Table 2**
Flow parameters and drag reduction of scleroglucan solutions.

| Scleroglucan concentration, $c$ % (w/w) | Reynolds number, $\rho U_B D / \eta_W$ | $U_B$ (m/s) | $u_\tau$ ($\equiv \sqrt{\tau_W / \rho}$) (m/s) | Drag reduction (%) $(f_N - f_P)/f_N \times 100$ |
|---|---|---|---|---|
| 0.005 | 31,000 | 0.38 | 0.019 | 13 |
| | 65,000 | 0.76 | 0.035 | 15 |
| | 109,000 | 1.26 | 0.053 | 17 |
| 0.01 | 36,000 | 0.50 | 0.024 | 24 |
| | 67,000 | 0.88 | 0.038 | 25 |
| | 97,000 | 1.01 | 0.043 | 27 |
| 0.02 | 35,000 | 0.05 | 0.023 | 37 |
| | 67,000 | 1.01 | 0.040 | 39 |
| | 75,000 | 1.14 | 0.044 | 40 |
| 0.05 | 33,000 | 0.63 | 0.026 | 40 |
| | 69,000 | 1.14 | 0.042 | 43 |
| | 78,000 | 1.26 | 0.047 | 42 |
| 0.075 | 31,000 | 0.76 | 0.030 | 47 |
| | 60,000 | 1.26 | 0.042 | 55 |

mer solution and the friction factor for water calculated at the same Reynolds number based on the Blasius approximation ($f = 0.079 Re^{-1/4}$), i.e.

$$DR(\%) = \left[ \frac{f_N - f_P}{f_N} \right] \times 100 \qquad (7)$$

where the subscripts $N$ and $P$ refer to the Newtonian fluid, and the polymer solution, respectively. We note that other methods of quantifying the degree of drag reduction are also available such as at the same Reynolds number based on the friction velocity (e.g. Escudier et al. [8]) and to a certain extent quantification of the "degree" of drag reduction is somewhat arbitrary. However, regardless of definition, the differences are small.

The degree of drag reduction for all concentrations studied, as seen from Fig. 6 and documented in Table 2, is a strong function of concentration but only weakly dependent on the Reynolds number, at least in the range measured here, in marked contrast to the data for flexible polymers (Virk [2], Ptasinski et al. [33], Escudier et al. [19]).

## 5. Mean flow and turbulence statistics

Mean axial velocity and complete Reynolds normal stress data, i.e. $u'$, $v'$ and $w'$, were measured at three different Reynolds numbers, all in the turbulent-flow regime for both 0.005% and 0.01% SG. Only one component of velocity could be obtained at any one time due to the refraction of two beam pairs of different wavelengths at the curved surface of the pipe wall resulting in the measuring volumes of the beam pairs occupying different spatial locations. As a consequence, it was not possible to measure the Reynolds shear stress, $\overline{u'v'}$. LDA measurements for higher concentrations were not possible due to the higher opacity of the solutions. Control runs with a Newtonian fluid, also within the turbulent-flow regime at approximately identical Reynolds numbers, were also performed as a basis for comparison.

### 5.1. Mean flow

The mean flow data is shown in wall coordinates (i.e. $u^+$ against $y^+$) in Fig. 7. For the Newtonian fluid, good agreement is observed with the well-known log law (see e.g. Tennekes and Lumley [34]). The data close to the wall are also in good agreement with that expected for the viscous sublayer (i.e. ($y^+ \leq 10$) $u^+ = y^+$). The SG data in the viscous sublayer also follow $u^+ = y^+$ while in the Newtonian core region, the data are shifted upward from, but remain

essentially parallel to, the Newtonian data as expected for low drag-reducing flows ([7,19]). The onsets of the shifts of the SG data were found to be independent of Reynolds number, occurring at a constant $y^+$ location of about 15. In physical units, this implies that the distance of onset location from the wall decreases with increasing Reynolds number. The magnitude of the shifts is a function of drag reduction but is only mildly dependent on Reynolds number.

### 5.2. Turbulence structure

The RMS fluctuation levels of the axial velocity $u'$, again plotted in wall coordinates, $u'^+(y^+)$, and shown in Fig. 8, show that closer to the wall ($y^+ < 30$), the water data collapse and are independent of the Reynolds number, in agreement with the observations of den Toonder and Nieuwstadt [18]. Closer to the pipe centreline there are clear Reynolds number trends, again in agreement with previous results [18]. Compared to the data for a Newtonian fluid at the same Reynolds number, both concentrations of SG showed increased values of $u'^+$ close to the wall with the location of the peaks found to be within the region of the onset of the shifts in the mean velocity profiles ($y^+ \approx 15$), i.e. in the buffer region. Close to the pipe centre the fluctuation levels are essentially identical to the water data at comparable Reynolds numbers.
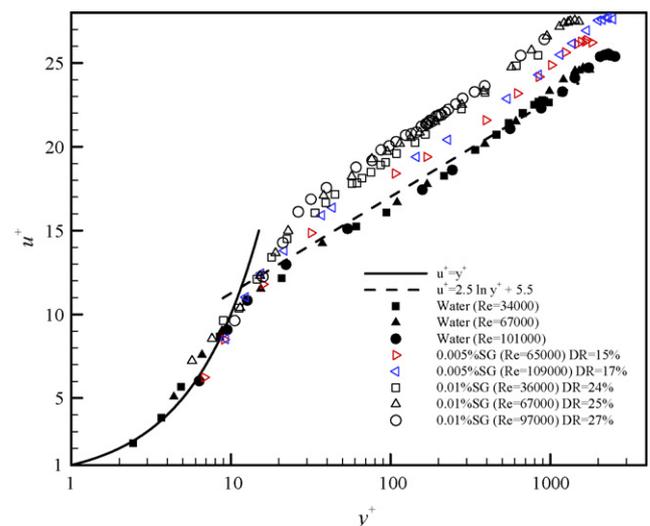


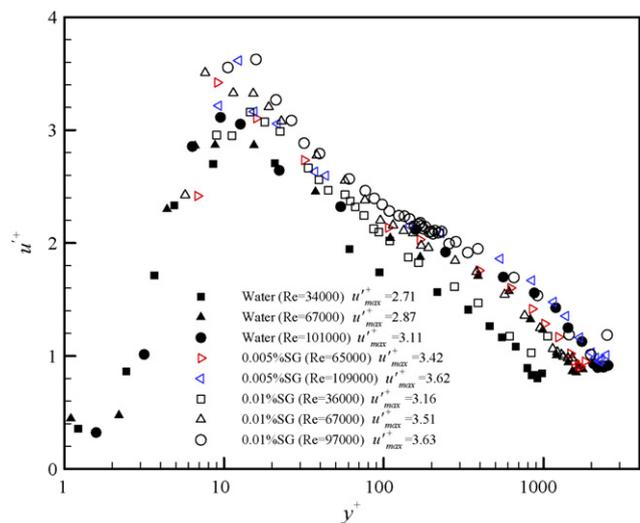**Fig. 7.** Universal mean velocity distribution for water, 0.005% SG and 0.01% SG.

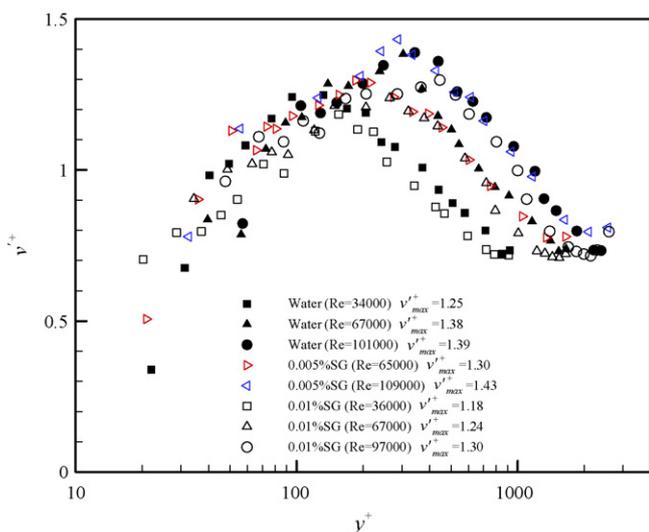**Fig. 8.** Axial turbulence intensities in wall coordinate for water, 0.005% SG and 0.01% SG.



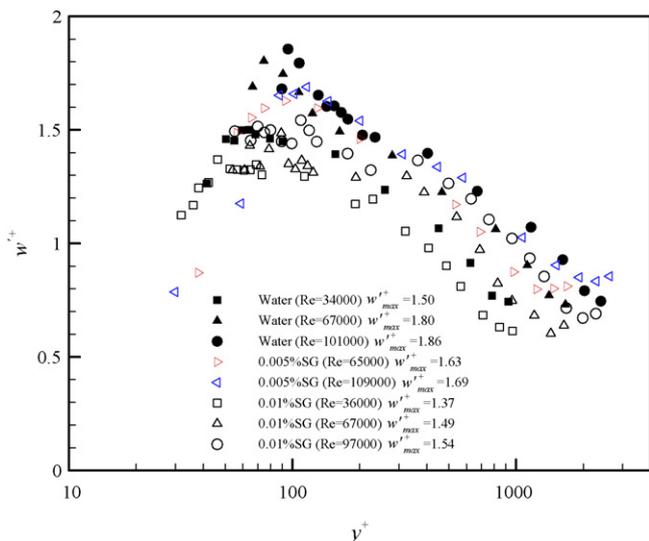**Fig. 9.** Radial turbulence intensities in wall coordinate for water, 0.005% SG and 0.01% SG.



**Fig. 10.** Tangential turbulence intensities in wall coordinate for water, 0.005% SG and 0.01% SG.
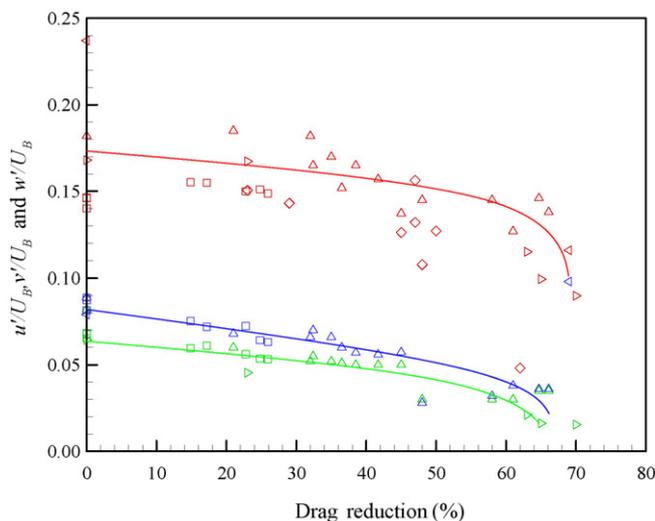


**Fig. 11.** Peaks of axial, radial and tangential fluctuation components normalized with the bulk velocity, $U_B$, against drag reduction (□: current study, △: PAA, XG, CMC (Presti [22]), ▷: HPAM (Ptasinski et al. [33]), ◁: Macro Fibres (McComb and Chan [35]), ◇: PEO, PAA (Allan et al. [36]), red: $u'/U_B$, green: $v'/U_B$, blue: $w'/U_B$). (For interpretation of the references to colour in this figure legend, the reader is referred to the web version of the article.)

Figs. 9 and 10 show that the RMS radial and tangential turbulent fluctuations for the Newtonian solvent are globally much lower than for the axial component, but exhibit increases with Reynolds number with the peaks situated further away from the wall. The SG results show increased suppression of the tangential and radial fluctuation levels with drag reduction with the exception of the peak of the radial fluctuation level at the highest Reynolds number measured for 0.005% SG.

In Fig. 11, the peak values of the turbulent fluctuation components, normalized with the bulk velocity, have been plotted against drag reduction together with selected data from the literature for comparison (Presti [22], Ptasinski et al. [33], McComb and Chan [35], Allan et al. [36], Chung and Graebel [37], Mizushina
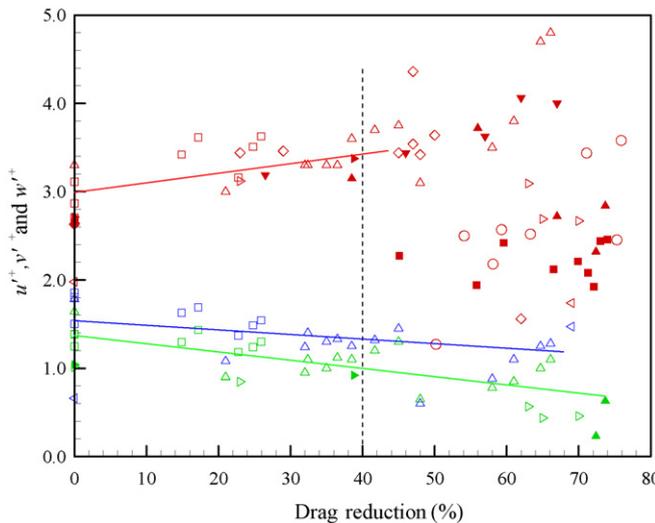


**Fig. 12.** Peaks of axial, radial and tangential fluctuation components in the wall coordinates against drag reduction (□: current study, △: PAA, XG, CMC (Presti [22]), ▷: HPAM (Ptasinski et al. [33]), ◁: Macro Fibres (McComb and Chan [35]), ◇: PEO, PAA (Allan et al. [36]), ○: PEO, PAA (Chung and Graebel [37]), ■: PEO (Mizushina and Usui [38]), ▲: PAA (Schummer and Thielen [39]), ▼: PEO (McComb and Rabie [40]), ▶: PAA (den Toonder et al. [41]), red: $u'^+$, green: $v'^+$, blue: $w'^+$). (For interpretation of the references to colour in this figure legend, the reader is referred to the web version of the article.)

and Usui [38], Schummer and Thielen [39], McComb and Rabie [40] and den Toonder et al. [41]). It can be seen that the data for the rigid-rod-like polymer from the current study agree well with the trend of decreasing normalized peaks with increasing drag reduction, similar to what is observed for two-dimensional channel flow [8]. In Fig. 12 the same data are plotted with the peak values are now normalized with the friction velocity, $u_\tau$, and the trend is for a decrease in the radial and tangential peak levels but an increasing trend of axial peak level below 40% drag reduction with more complex behaviour at higher drag reduction. The lines in figures are included to guide the eye where clear trends are apparent.

## 6. Conclusions

The data presented here confirm that so-called rigid, rod-like polymer solutions, in our case a scleroglucan, are effective as drag-reducing agents. The drag reduction effectiveness increases as the solution concentration is increased and is only mildly dependent on Reynolds number but is still relatively lower than that for flexible polymer solutions. The mean axial and turbulence structure data exhibit behaviour typical of a low drag-reducing flexible polymer solution such as carboxymethylcellulose with increases in $u'^+$ and decreases both in $w'^+$ and $v'^+$ generally, except for 0.005% SG at the highest Reynolds number. It is suggested that in order to fully understand the mechanism of drag reduction for such rigid-rod polymer solutions, for example whether the same mechanism for a flexible polymer applies to rigid-rod polymers, direct numerical simulations using suitable constitutive equations will play a key role. Our aim with the current results is to provide an experimental database of low-order statistics to assist in the validation of such simulations and guide the development of turbulence modelling.

## References

[1] J.L. Lumley, Drag reduction in turbulent flow by polymer additives, J. Polym. Sci. Macromol. Rev. 7 (1973) 263–290.
[2] P.S. Virk, Drag reduction fundamentals, AIChE J. 21 (4) (1975) 625–653.
[3] N.S. Berman, Drag reduction by polymers, Ann. Rev. Fluid Mech. 10 (1978) 47–64.
[4] J.W. Hoyt, Drag reduction, Encyclopedia of Polymer Science and Engineering, vol. 5, Wiley, New York, 1986, pp. 129–151.
[5] F.T.M. Nieuwstadt, J.M.J. den Toonder, Drag reduction by additives: a review, in: A. Soldati, R. Monti (Eds.), Turbulence Structure and Motion, Springer Verlag, 2001, pp. 269–316 (Book Chapter).
[6] M.D. Graham, Drag reduction in turbulent flow of polymer solutions, in: D.M. Binding, K. Walters (Eds.), Rheology Reviews, British Society of Rheology, 2004, pp. 143–170.
[7] M.D. Warholic, H. Massah, T.J. Hanratty, Influence of drag-reducing polymers on turbulence: effects of Reynolds number, concentration and mixing, Exp. Fluids 27 (1999) 461–472.
[8] M.P. Escudier, A.K. Nickson, R.J. Poole, Turbulent flow of viscoelastic shear-thinning liquids through a rectangular duct: Quantification of turbulence anisotropy, J. Non-Newtonian Fluid Mech 160 (2009) 2–10.
[9] J.S. Paschkewitz, Y. Dubief, E.S.G. Shaqfeh, The dynamic mechanism for turbulent drag reduction using rigid fibers based on Lagrangian conditional statistics, Phys. Fluids 17 (2005), 063102-1-18.
[10] N.S. Berman, Evidence for molecular interactions in drag reduction in turbulent pipe flows, Polym. Eng. Sci. 20 (7) (1980) 451–455.
[11] H.W. Bewersdorff, R.P. Singh, Rheological and drag reduction characteristics of xanthan gum solutions, Rheol. Acta 27 (1988) 617–627.
[12] S. Sasaki, Drag reduction effect of rod-like polymer solutions. I. Influence of polymer concentration and rigidity of skeletal back bone, J. Phys. Soc. Jpn. 60 (3) (1991) 868–878.
[13] P.S. Virk, D.C. Sherman, D.L. Wagger, Additive equivalence during turbulent drag reduction, AIChE J. 43 (12) (1997) 3257–3259.
[14] R. Benzi, E.S.C. Ching, T.S. Lo, V.S. L'vov, I. Procaccia, Additive equivalence in turbulent drag reduction by flexible and rodlike polymers, Phys. Rev. E 72 (2005) 016305.
[15] J.S. Paschkewitz, Y. Dubief, C.D. Dimitropoulos, E.S.G. Shaqfeh, P. Moin, Numerical simulation of turbulent drag reduction using rigid fibres, J. Fluid Mech. 518 (2004) 281–317.
[16] R. Benzi, E.S.C. Ching, E.D. Angelis, I. Procaccia, Comparison of theory and direct numerical simulations of drag reduction by rodlike polymers in turbulent channel flows, Phys. Rev. E77 (2008) 046309.
[17] J.J.J. Gillissen, B.J. Boersma, P.H. Mortensen, H.I. Anderson, Fibre-induced drag reduction, J. Fluid Mech. 602 (2008) 209–218.
[18] J.M.J. den Toonder, F.T.M. Nieuwstadt, Reynolds number effects in a turbulent pipe flow for low to moderate Re, Phys. Fluids 9 (11) (1997) 3398–3408.
[19] M.P. Escudier, F. Presti, S. Smith, Drag reduction in turbulent pipe flow of polymers, J. Non-Newtonian Fluid Mech. 81 (1999) 197–213.
[20] P. Buchhave, W.K. George, J.L. Lumley, The measurements of turbulence with the laser-Doppler anemometer, Ann. Rev. Fluid Mech. 11 (1979) 443–503.
[21] A.F. Bicen, Refraction correction for LDA measurements in flows with curved optical boundaries, TSI Quater. VII (2) (1982) 10–12.
[22] F. Presti, Investigation of transitional and turbulent pipe flow of non-Newtonian fluids, PhD thesis, University of Liverpool, 2000.
[23] C. Tropea, Laser Doppler anemometry: recent developments and future challenges, Meas. Sci. Technol. 6 (1995) 605–619.
[24] W.J. Yanta, R.A. Smith, Measurements of turbulence-transport properties with a laser Doppler velocimeter, AIAA 11th Aerospace Science Meeting, 1973.
[25] R. Lapasin, S. Pricl, Rheology of Industrial Polysaccharides: Theory and Applications, Blackie Academic and Professional, 1995.
[26] K. Yasuda, R.C. Armstrong, R.E. Cohen, Shear flow properties of concentrated solutions of linear and star branched polystyrenes, Rheol. Acta 20 (1981) 163–178.
[27] M.P. Escudier, I.W. Gouldson, A.S. Pereira, F.T. Pinho, R.J. Poole, On reproducibility of the rheology of shear-thinning liquids, J. Non-Newtonian Fluid Mech. 97 (2001) 99–124.
[28] W.E. Rochefort, S. Middleman, Rheology of xanthan gum: salt, temperature, and strain effects in oscillatory and steady shear experiments, J. Rheol. 31 (4) (1987) 337–369.
[29] H. Lee, Rheology of concentrated isotropic and anisotropic rigid polysaccharide solutions: xanthan and scleroglucan, PhD thesis, University of California, USA, 2001.
[30] L.E. Rodd, T.P. Scott, J.J. Cooper-White, G.H. McKinley, Capillary break-up rheometry of low-viscosity elastic fluids, Appl. Rheol. 15 (2005) 12–27.
[31] M. Stelter, G. Brenn, Elongational rheometry for the characterization of viscoelastic fluid, Chem. Eng. Technol. 25 (1) (2002) 30–35.
[32] E. Pelletier, C. Viebke, J. Meadows, P.A. Williams, A rheological study of the order-disorder conformational transition of xanthan gum, Biopolymers 59 (2001) 339–346.
[33] P.K. Ptasinski, F.T.M. Nieuwstadt, B.H.A.A. Van Den Brule, M.A. Hulsen, Experiments in turbulent pipe flow with polymer additives at maximum drag reduction, Flow Turbul. Combust. 66 (2001) 159–182.
[34] H. Tennekes, J.L. Lumley, A First Course in Turbulence, The MIT Press, 1972.
[35] W.D. McComb, K.T. Chan, Laser Doppler anemometer measurements of turbulent structure in drag reducing fibre suspensions, J. Fluid Mech. 152 (1985) 455–478.
[36] J.J. Allan, C.A. Greated, W.D. McComb, Laser Doppler anemometer measurements of turbulent structure in non-Newtonian fluids, J. Phys. D: Appl. Phys. 17 (1984) 533–549.
[37] J.S. Chung, W.P. Graebel, Laser anemometer measurements of turbulence in non-Newtonian pipe flows, Phys. Fluids 15 (4) (1971) 546–554.
[38] T. Mizushina, H. Usui, Reduction of eddy diffusion for momentum and heat in viscoelastic fluid flow in a circular tube, Phys. Fluids 20 (10) (1977) s100–s108.
[39] P. Schummer, W. Thielen, Structure of turbulence in viscoelastic fluids, Chem. Eng. Commun. 4 (4–5) (1980) 593–606.
[40] W.D. McComb, L.H. Rabie, Local drag reduction due to injection of polymer-solutions into turbulent-flow in a pipe. 1. Dependence on local polymer concentration, AIChE J. 28 (4) (1982) 547–557.
[41] J.M.J. den Toonder, M.A. Hulsen, G.D.C. Kuiken, F.T.M. Nieuwstadt, Drag reduction by polymer additives in a turbulent pipe flow: numerical and laboratory experiments, J. Fluid Mech. 337 (1997) 193–231.